or

$$G(\eta) = (d\theta/d\xi)(1/\theta)(x - \xi) \tag{A6}$$

where

$$G(\eta) = \int_{\eta_0}^{\eta} F_1(\eta')d\eta'$$

From Eq. (A6), we obtain

$$\partial G/\partial x = (dG/d\eta)\partial\eta/\partial x = (d\theta/d\xi)1/\theta \tag{A7a}$$

and

$$\frac{\partial G}{\partial \xi} = \frac{dG}{d\eta}\frac{\partial \eta}{d\xi} = (x - \xi)\left(\frac{d^2\theta}{d\xi^2}\cdot\frac{1}{\theta} - \frac{(d\theta/d\xi)^2}{(\theta)^2}\right) - \frac{d\theta}{d\xi}\frac{1}{\theta} \tag{A7b}$$

After these expressions are inserted in Eq. (A4b), and assuming that $dG/d\eta \neq 0$, we arrive at

$$\left[(x - \xi)\left(\frac{d^2\theta}{d\xi^2}\frac{1}{\theta} - \frac{(d\theta/d\xi)^2}{\theta^2}\right) - \frac{d\theta}{d\xi}\cdot\frac{1}{\theta}\right] = F_2(\eta)\frac{d\theta}{d\xi}\frac{1}{\theta} \tag{A8}$$

Using Eq. (A6), this can be written as

$$\left[G(\eta)\frac{\theta_{\xi\xi}}{\theta_\xi}\frac{\theta}{\theta_\xi}\right] = F_2(\eta) + 1 + G(\eta) \tag{A9a}$$

or

$$\frac{\theta_{\xi\xi}}{\theta_\xi}\frac{\theta}{\theta_\xi} = \frac{F_2(\eta) + 1 + G(\eta)}{G(\eta)} \tag{A9b}$$

For this to be true, it is necessary that

$$\frac{\theta_{\xi\xi}}{\theta_\xi}\frac{\theta}{\theta_\xi} = \lambda \tag{A10}$$

where λ is a constant. Then, after integrating,

$$\theta_\xi = a\theta^\lambda \tag{A11}$$

where a is a constant. If $\lambda \neq 1$,

$$\theta = A\{\xi + B\}^{1/1-\lambda} \tag{A12}$$

where A and B are constants. The case $\gamma = 1$ clearly corresponds to the exponential shock wave [from Eq. (A11)], and the case $\gamma \neq 1$ corresponds to the power law shock wave.

References

[1] Hayes, W. D. and Probstein, R. F., "Hypersonic Flow Theory," Vol. 1, *Inviscid Flow*, 2nd ed., Academic Press, New York, 1966, p. 167.

[2] Mirels, H., "Hypersonic Flow Over Slender Bodies Associated With Power-Law Shocks," *Advances in Applied Mechanics*, Vol. VII, edited by H. L. Dryden and T. von Kármán, Vol. VII, Academic Press, New York, 1962, pp. 1–54.

[3] Chernyi, G. G., *Introduction to Hypersonic Flow*, Academic Press, New York, 1961.

[4] Cole, J. D., "Newtonian Flow Theory for Slender Bodies," *Journal of the Aeronautical Sciences*, Vol. 24, 1957, pp. 448–455.

[5] Cole, J. D. and Aroesty, J., "Optimum Hypersonic Lifting Surfaces Closer to Flat Plates," *AIAA Journal*, Vol. 3, No. 8, Aug. 1965, pp. 1520–1522.

[6] Cole, J. D. and Aroesty, J., "Hypersonic Similarity Solutions for Airfoils Supporting Exponential Shock Waves," RM-5724-PR, Aug. 1968, The RAND Corp.

FEBRUARY 1970 AIAA JOURNAL VOL. 8, NO. 2

Cone Drag in Rarefied Hypersonic Flow

M. I. Kussoy* and C. C. Horstman*
NASA Ames Research Center, Moffett Field, Calif.

Experimental drag coefficients for spheres and sharp cones in rarefied hypersonic air flow are presented. These data were obtained using a free-flight technique in a shock tunnel. The test conditions were Mach number from 15 to 24.6, Reynolds number/in. from 690 to 2630, mean free path from 0.009 to 0.053 in., and cone semivertex angles from 2.5° to 25°. When compared with hypersonic viscous interaction and near free molecular theories (both computed for the present range of test conditions), the cone drag is overestimated. However, applying the viscous interaction parameter of Mirels and Ellinwood, a correlation of cone drag for each cone angle in terms of Mach number and freestream Reynolds number is developed. A correlation of average local skin-friction coefficient (deduced from the present data) for individual cone angles is also developed in terms of Mach number and freestream Reynolds number. The ratio of skin-friction to heat-transfer coefficient is shown to be a function only of cone angle.

Nomenclature

C = Chapman-Rubesin viscosity law coefficient ($\mu_w T/\mu T_w$)
C_D = drag coefficient referenced to base area
C_H = Stanton number
$\bar{c}_f$ = average local skin-friction coefficient
Kn = Knudsen number
l = axial length of model
M = Mach number
q = dynamic pressure
Re = Reynolds number
T = temperature
U = velocity
λ = mean free path
θ_c = cone semivertex angle
μ = viscosity

Subscripts

D = diameter
INV = inviscid

Presented as Paper 69-140 at the AIAA 7th Aerospace Sciences Meeting, New York, January 20–22, 1969; submitted February 3, 1969; revision received May 23, 1969.

* Research Scientist. Member AIAA.

l = axial length of model
w = wall value
x = distance along model axis from apex
0 = stagnation value
2 = value behind normal shock
∞ = freestream value

Introduction

INVESTIGATIONS of hypersonic rarefied flow over sharp bodies have indicated the existence of a spectrum of regimes between the flow at the tip and the classical boundary-layer flow far downstream. Proceeding from the cone apex, these regimes can be divided into noncontinuum flow, merged-layer flow, strong and/or weak interaction, and classical boundary-layer flow. Most of the experimental and theoretical work in the last few years has been concentrated on the flowfield and surface properties near the leading edge of sharp flat plates. Relatively few investigations have been performed in the noncontinuum and merged-flow regime on axisymmetric bodies, where the added factor of transverse curvature is present. Limited surface pressure[1] and heat-transfer[2,3] measurements have been obtained in these flow regimes. Previous drag measurements[4,5] (with the exception of Geiger[6]) have been obtained in a regime where merged layer flow as opposed to noncontinuum flow was dominant. However, there has been no systematic study of the effects of freestream Mach number, Reynolds number, mean free path, or cone angle on the drag of slender cones where noncontinuum flow covers a significant portion of the cone.

In this paper, the primary attention will be focused on the drag of sharp cones completely immersed in the noncontinuum and merged-flow regimes. There are theories that predict drag in the noncontinuum[7-9] and viscous interaction[10-12] regimes. To date, there has been no verification between theory and experiment in the noncontinuum regime. In addition, the extension of the viscous-interaction theories into the merged-flow regime has not been experimentally verified.

The purpose of the present investigation was to ascertain the influence of Mach number, M_∞, Reynolds number, Re_∞, mean free path, λ_∞, and cone semivertex angle, θ_c, on the experimental drag of cones in the noncontinuum and merged-flow regimes. These data should provide the important flow parameters in this regime, as well as indicate the validity of the noncontinuum theories and any extension of available theories into the merged-flow regime.

Experimental Procedure

Facility and Test Conditions

The tests were performed in the Ames 42-in. shock tunnel. The test medium, air, was expanded through a 9-ft. long, 10°-half-angle conical nozzle into a 42-in.-wide hexagonal test section. The general operation of the tunnel has been reported in Refs. 13 and 14. The procedure used to determine the test-section conditions from measurements in the driver tube, reservoir, and test section is discussed in detail in Ref. 15. Briefly, from the measured shock velocity in the driven tube, total enthalpy was computed (4000 Btu/lbm). Test section Pitot and static pressures as well as reservoir pressure were measured, and these data, used in conjunction with a one-dimensional nozzle expansion computer program discussed in Ref. 15, determined the effective area ratio and the Mach number at which the flow froze. This value of freeze Mach number was 3.8 (both vibrational and chemical freezing) for the three selected throat diameters (0.1, 0.2, and 0.4 in.). These data determined the other flow conditions given in Table 1. The dynamic pressure determined from the measured drag of a sphere of known drag coefficient agreed within 10% with the values computed from the expansion program for these test conditions. Flow uniformity was determined by simultaneously running several spheres of the same diameter and mass at different positions in the test core. The measured variation in drag (and thus dynamic pressure) between them was a maximum of 7%. This variation was of the same order ($\sim$10%) as the measured run to run variation in dynamic pressure normalized by the measured reservoir pressure. A 10% change in normalized dynamic pressure resulted in a computed change[15] in M_∞ of 3% and Re_∞ of 7%. Since the run to run variation in test conditions were of the same order as the flow gradients within any particular run, the nominal conditions were used for the presentation of the experimental results. The tunnel run time was approximately 15 msec.

Models

The test models were sharp cones with semivertex angles of 2.5°, 5°, 10°, and 25°. In order to obtain a Reynolds number variation, the models had different lengths. To insure a reasonable static-stability margin, the model nose was made of aluminum or magnesium, and the base of light wood, such as pine or balsa. These two materials were first glued together and then machined. The model tips were approximately 0.001 in. in diameter, and thus were considered sharp for aerodynamic purposes since the mean free path, λ_∞, varied from 0.009 to 0.053 in.

Test Procedure and Instrumentation

A free-flight technique was used for measuring the drag. This method was used for the following reasons. In order to obtain drag in the highly rarefied flow regime, using the test conditions shown in Table 1, small models had to be tested. Even though force balances have been designed to measure the small forces (a minimum of 100 mg) on models of this size, the interference effects on these small models from the balance and associated sting are unknown. In order to insure that the drag data obtained were free of sting interference effects, the free-flight technique was used. This method is similar to that described in Ref. 4. A sketch of a typical run setup for the present investigation is shown in Fig. 1. Several cone models and a calibrating sphere (sphere of known drag coefficient) were suspended from a frame in the test section by means of silk threads, $\frac{1}{2}$ mil in diameter. The initial starting shock burned these threads in approximately 1 msec, leaving the models, which were at room temperature throughout the entire run, suspended in the test section. Two high-speed 16-mm cameras, operating at 500 frames/sec, recorded the flight of the models (see Fig. 1). The upper camera was used to monitor the angle of attack of the models in the plane 60° from the pitch plane. Yaw angles computed using the data from both cameras were usually less than $\pm 1°$. In some cases, however, the two threads holding the cone models burned unequally, causing the model to pitch to an initial angle of attack. Drag data from cones that pitched to an average angle of attack greater than 4°, or greater than the cone semivertex angle, were discarded. Using this criteria, it was found that the drag data for a given model configuration (θ_c and length) obtained under a given set of test conditions were independent of angle of attack.

Data Reduction and Precision

The cone-drag coefficient, C_D, was obtained by dividing the product of model mass and acceleration by the tunnel dynamic pressure, q_∞, and referencing the result to the cone base area. The acceleration was determined by fitting straight line slopes to distance vs time-squared curves. These curves were obtained from enlarged prints of the film data by measuring the distances traversed by the models and knowing the subsequent time between film frames. Absolute distances were obtained by taking into account the relative position of the model, camera, and reference grid.

Table 1 Nominal running conditions for the 42-in. shock tunnel

Condition	M_∞	Re_∞/in.	Re_2/in.	T_∞, °R	λ_∞, in.	U_∞, fps
1	24.6	694	24	118	0.053	13,725
2	19.0	1246	76	213	0.023	13,680
3	15.0	2627	244	341	0.009	13,630

In order to insure that the tunnel was operating properly, a calibrating sphere was flown along with the cone models in each run. (It was felt that this calibrating sphere would provide less flow disturbance than the large Pitot probe and its associated sting.) In addition, since the normalized dynamic pressure did vary between runs, the calibrating sphere was also used to determine q_∞. The drag coefficients of the calibrating spheres were determined from tests similar to those described previously. Spheres of various diameter were run simultaneously with a large sphere of known drag coefficient for each test condition. These known drag coefficients were obtained from previously published correlations of high Reynolds numbers sphere-drag data.[4,16–18] Thus, knowing the calibrating sphere-drag coefficient, model acceleration, and model mass, q^1 could be calculated for a particular test. In all cases the normalized dynamic pressure determined from the calibrating sphere was within 10% of the computed nominal test conditions.

The sphere-drag data are presented in Table 2 and compared with previously published data[4,16–18] in Fig. 2. Only data extending from the large Reynolds number limit ($C_D \approx 0.9$) were used for this comparison. There is general agreement among all data, with the present results having the least scatter.† This agreement is a good indication of the validity of the test technique, as well as the accuracy of the data which have been calculated to be ±10% for the present investigation.

Table 2 Sphere drag-coefficient results

Sphere diam, in.	C_D
Condition 1: $M_\infty = 24.6$, $T_w = 530$°R	
5.5	1.04
3.0	1.12
1.5	1.42, 1.52
0.4	1.64
0.3	2.07
0.25	2.02
0.2	2.13, 2.08
0.15	2.04
0.1	2.02
0.094	2.38
0.05	2.22
Condition 2: $M_\infty = 19.0$, $T_w = 530$°R	
5.5	0.92
3.0	1.01
1.0	0.99, 1.12
0.5	1.27
0.4	1.39
0.3	1.50, 1.53
0.25	1.62
0.2	1.62, 1.56, 1.66, 1.5
0.15	1.79
0.1	1.64
0.094	1.81, 1.79, 1.78
0.065	1.80
Condition 3: $M_\infty = 15$, $T_w = 530$°R	
3.0	0.90
0.5	1.04, 0.98
0.4	0.97
0.3	1.00
0.25	1.15, 1.12
0.2	1.13
0.15	1.23, 1.24, 1.20
0.1	1.31, 1.30
0.05	1.60, 1.66

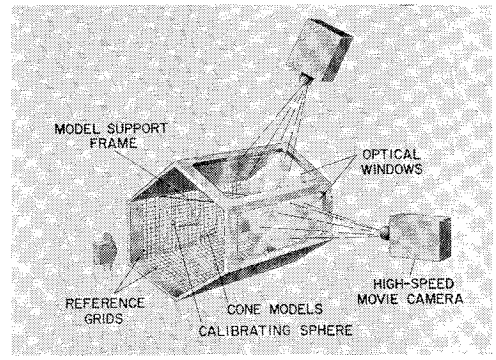

Fig. 1 Typical test-section arrangement in the Ames 42-in. shock tunnel.

Results and Discussion

In this section, several theories that predict cone drag will be briefly reviewed, and then the drag data will be presented and compared with these theories. Finally, the local skin-friction coefficient, deduced from the drag data, will be presented and compared with theory.

Theories

There is no single theory currently available that can be used to predict the drag coefficients for sharp cones over the range from the free molecule to the inviscid flow regime. In the theories presented in this section, certain assumptions have been made in the formulation which limit the range of flow conditions for which these theories apply. For the region very close to the cone apex (i.e., the near-free molecular regime), Laurmann[8] reworked Kogan's[7] general formula for C_D, which was obtained by considering only the effects of first collisions. Also, for this near-free molecular flow regime, Ortloff[9] used restricted variational method to solve the Boltzmann equation, but only presented solutions for $\theta_c = 5°$ and

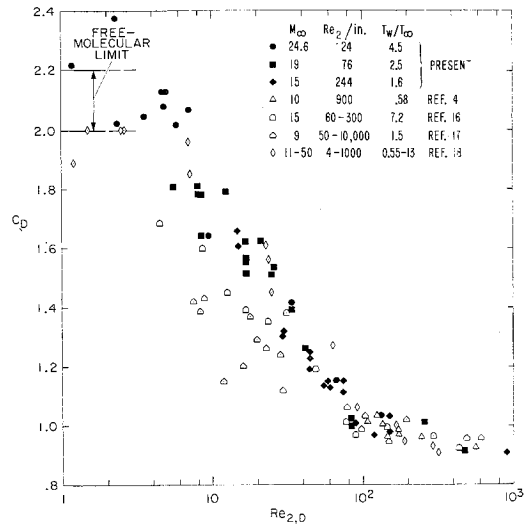

Fig. 2 Sphere-drag-coefficient variation with Reynolds number.

† The sphere data in Ref. 4 taken at $M_\infty \approx 14$ are suspected of being in error, since they are about 20% higher than three other sets of data taken in the same flow conditions. For this reason, they are not shown in the preceding comparison.

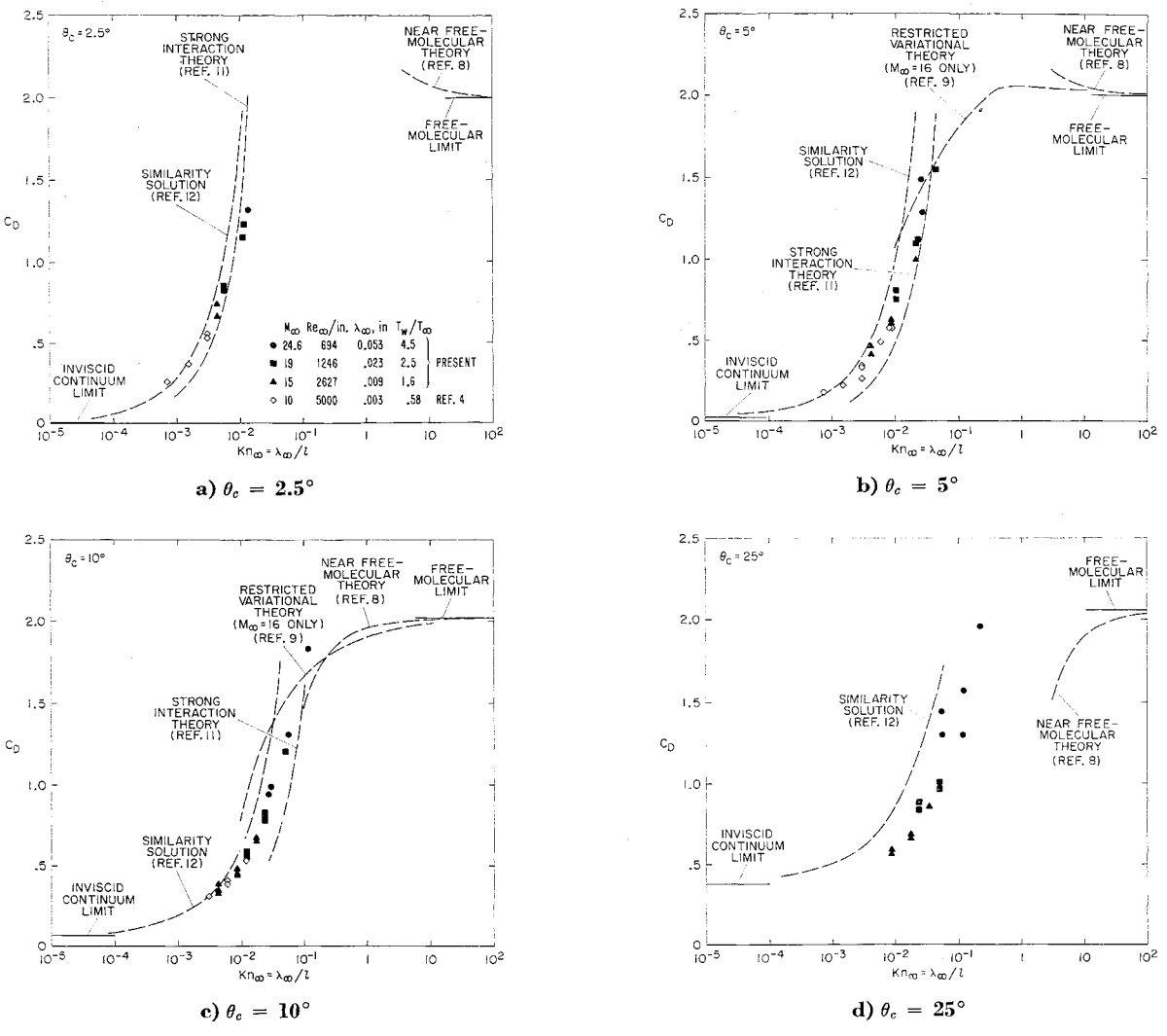

Fig. 3 Variation of cone-drag coefficient with Knudsen number in the noncontinuum and merged-flow regimes.

10° and $M_\infty = 16$. Far downstream from the apex, in the boundary-layer interaction regime (i.e., where Rankine-Hugoniot shock-wave relations hold), Ellinwood and Mirels[11] have recently extended Stewartson's[10] original strong-interaction solution to include a power-law viscosity variation and variable Prandtl number; this solution is valid in the limit of the viscous-interaction parameter, $M_\infty (C_\infty/Re_\infty, l)^{1/2}/\sin^2\theta_c$, approaching ∞. In addition, Mirels and Ellinwood[12] obtained a similarity solution, valid from the weak-interaction regime to the strong-interaction regime. These two viscous interaction theories[11,12] do not take into account shock-wave boundary-layer merging which is known to occur over a significant portion of the present test bodies.[19] For all these theoretical computations, the cone base pressure was assumed to be equal to the freestream static pressure, and the inviscid drag was computed using an inviscid characteristics solution.[20]

Drag

The cone drag results are presented in Figs. 3a–d, and also given in Table 3. The drag coefficients, C_D, are plotted against the freestream Knudsen number, Kn_∞, for semivertex angles, θ_c, of 2.5°, 5°, 10°, and 25°. The limits of C_D for inviscid and free-molecule flow for each θ_c are also given for reference. (The free-molecule limit was computed from Ref. 21, assuming diffuse reflection and an accommodation coefficient of unity, and is only for the higher Mach number condition.) For the range of M_∞, Re_∞/in. and λ_∞ of the present investigation the data fall in a very narrow band for each cone angle, and rise steeply toward the free-molecule limit with increasing Kn_∞. Shown for comparison are previously published data from Ref. 4 obtained at $M_\infty \approx 10$.‡ These previous data agree reasonably well with the present results.

The theories previously discussed have been computed for the present range test conditions, where possible, and compared with the data in Fig. 3. Note that it is indicated in Ref. 8 that for $\theta_c < 9°$, the predicted value of C_D is higher than the free-molecular value, and for $\theta_c > 9°$, it is lower. The fact that the present data fell below the similarity solution is consistent with previous merged-flow studies[1,19,22] which have shown substantial reductions in the values of the surface pressure and skin friction from those of the viscous-interaction predictions in this flow regime. None of the theories consistently predicts the drag results. However, for each cone angle, the general trend of the data is predicted by the viscous-interaction theories.[11,12] Therefore, in an attempt to correlate the viscous drag, the present data are replotted in the form suggested by these viscous interaction theories, for example, $[(C_D - C_{D,\,\mathrm{INV}})/C_{D,\,\mathrm{INV}}][(1 + 3.46\ T_w/T_o)/(1 + 0.23\ T_w/T_o)]$ vs $M_\infty(C_\infty/Re_\infty, l)^{1/2}/\sin^2\theta$.

Figure 4 represents a systematic presentation of the drag data as a function of freestream conditions, and clearly illustrates the inability of the viscous interaction parameters to correlate such drag data in the merged-layer and non-

‡ The cone data taken at $M_\infty \approx 14$ in Ref. 4 are not shown since they are directly related to the sphere drag data that were felt to be in error.

Table 3 Cone drag-coefficient results

θ_c, deg	Length, in.	C_D
Condition 1: $M_\infty = 24.6$, $T_w = 530°R$		
2.5	4.0	1.30
5.0	2.0	1.49, 1.28
10.0	0.5	1.83
	1.0	1.31
	2.0	0.94, 0.99
25.0	0.25	1.95
	0.5	1.57, 1.29
	1.0	1.29, 1.43
Condition 2: $M_\infty = 19.0$, $T_w = 530°R$		
2.5	2.0	1.15, 1.22
	4.0	0.85, 0.82
5.0	0.5	1.54
	1.0	1.12, 1.11
	2.0	0.80, 0.75
10.0	0.5	1.20
	1.0	0.81, 0.78, 0.83
	2.0	0.59, 0.56
25.0	0.5	1.00, 0.96
	1.0	0.83, 0.87
Condition 3: $M_\infty = 15.0$, $T_w = 530°R$		
2.5	2.00	0.66, 0.73
5.0	0.38	1.00
	1.00	0.62, 0.61
	2.00	0.41, 0.46
10.0	0.50	0.67, 0.67
	1.00	0.46, 0.46, 0.47
	2.00	0.35, 0.35, 0.39
25.0	0.25	0.84
	0.50	0.68, 0.67
	1.00	0.59, 0.56

continuum regimes. The data for each cone semivertex angle fall into a narrow band, which curves slightly toward the respective free molecular limit[21] as the interaction parameter is increased. Other published data[4–6] shown on this figure compare favorably with the present data. It is interesting to observe that Geiger's[6] 6° data fall about 15% below the present 5° data at high values of the viscous interaction parameter. This is approximately the same amount that the respective free molecular limits differ.

Also shown in Fig. 4 are the drag predictions of the similarity solution[12] and strong-interaction[11] theory. Neither of these theories consistently predicts the magnitude of the data. With the exception of the 25° cones, the similarity solution[12] defines the limit of the data when the boundary-layer interaction flow regime covers a significant part of the body (i.e., low values of the viscous-interaction parameter). The 25° data do not approach the similarity solution[12] since this theory is only valid for the viscous interaction parameter much greater than unity.

Skin Friction

Skin friction is a major portion of the drag of a slender cone in hypersonic rarefied flow.[4] Thus, it is of interest to study the variation of the skin-friction coefficient over the test bodies in the present investigation. The friction drag, and from this an average skin-friction coefficient, $\bar{c}_f$, was deduced by taking advantage of the fact that cones of various lengths were tested under the same flow conditions. This was done in the following manner. The pressure contribution to the drag was estimated from a recent experimental correlation of surface pressures on slender cones.[1] (This drag was found to be less than 10% of the total drag for the slender cones, $\theta_c = 2.5°$ to 10°.) Subtracting this pressure drag from the total drag resulted in the friction contribution to the drag. By choosing two cones of angle θ_c with different lengths and testing them under the same tunnel conditions, the friction drag (and

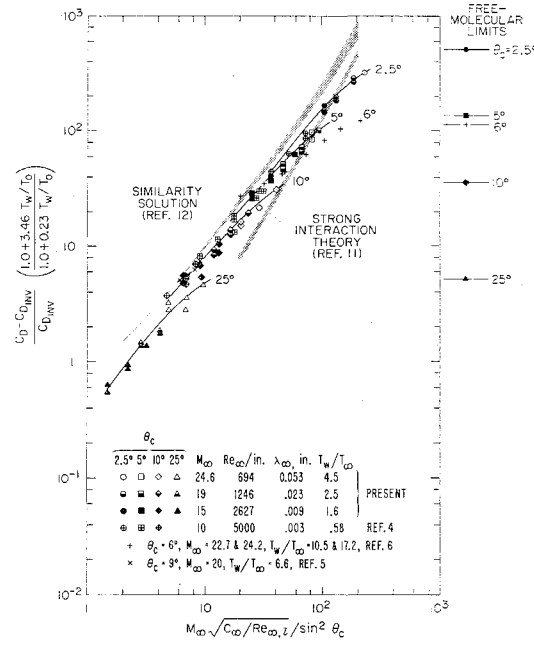

Fig. 4 Cone-drag-coefficient variation with the viscous-interaction parameter in the noncontinuum and merged-flow regimes for θ_c from 2.5° to 25°.

hence the average friction coefficient) acting on the cone frustum defined by the two lengths was found. This average local skin-friction coefficient, $\bar{c}_f$, was assumed to act at the centroid of area of the frustum. Since the lengths of cones used in these tests were 0.25, 0.5, 1.0, 2.0, and 4.0 in., the $\bar{c}_f$ values obtained represented average coefficients over lengths of 0.25, 0.5, 1.0, and 2.0 in.

The values of $\bar{c}_f$, as well as those deduced in a similar manner from the $M_\infty \approx 10$ data of Ref. 4, are plotted in Fig. 5 in the form suggested by the viscous-interaction theories,[11,12] that is, $\bar{c}_f/\sin^3\theta_c$ vs $M_\infty(C_\infty/Re_{\infty,x})^{1/2}/\sin^2\theta_c$. For each cone angle, the data fall within the shaded areas and smoothly approach the respective free-molecular values (diffuse reflection, accommodation coefficient of unity, and $M_\infty = 24.6$) as the viscous-interaction parameter increases. The similarity solution[12] and strong-interaction[11] theory are shown in this figure for comparison with the data. Though both theories do not consistently predict the magnitude of the data, the similarity solution defines the limit of the data (except for the 25° cone) as the viscous-interaction parameter becomes small.

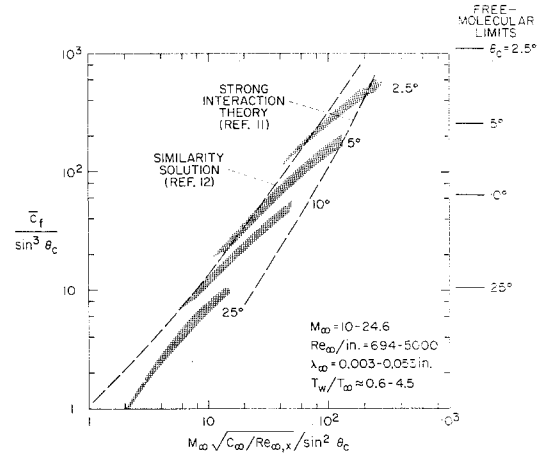

Fig. 5 Variation of average local skin-friction coefficient with the viscous-interaction parameter in the noncontinuum and merged-flow regimes for θ_c from 2.5° to 25°.

As a natural extension of the skin-friction results, the dependence of the Reynolds analogy factor, $\bar{c}_f/2C_H$, on the model geometry and test conditions can be deduced. A previous investigation[23] has shown that for conditions similar to those of the present work, the Stanton number, C_H, when plotted in the form $C_H/\sin^3\theta_c$ vs viscous-interaction parameter, is independent of θ_c for values of $M_\infty(C_\infty/Re_{\infty,x})^{1/2} < 0.6$. It has been shown above that for all values of $M_\infty(C_\infty/Re_{\infty,x})^{1/2}$, $\bar{c}_f/\sin^3\theta_c$ depends on θ_c and hence $\bar{c}_f/2C_H$ is a function of θ_c for the present range of test conditions. This result is similar to published results for hypersonic rarefied flow over wedges,[22] where $\bar{c}_f/2C_H$ can also be shown to be a function of wedge angle.

Conclusions

Free-flight drag measurements on sharp cones ($\theta_c = 2.5°$ to 25°) completely immersed in the noncontinuum and merged-flow regimes resulted in the following conclusions:

1) No available theories consistently predict the drag; however, using the viscous-interaction parameters of Mirels and Ellinwood,[12] drag data were correlated in terms of M_∞ and $Re_{\infty,l}$ for a given value of θ_c.

2) The average local skin friction, $\bar{c}_f$, deduced from the present drag data, was also found to correlate in terms of the viscous-interaction parameter for a given cone angle.

References

[1] Kussoy, M. I. and Horstman, C. C., "An Experimental Study of Hypersonic Rarefied Flow Over Sharp Cones," *Proceedings of the Sixth Rarefied Gas Dynamics Symposium*, Boston, Mass., 1968, to be published.

[2] Wilkinson, D. B. and Harrington, S. A., "Hypersonic Force, Pressure, and Heat Transfer Investigations of Sharp and Blunt Slender Cones," TDR-63-177, Aug. 1963, Arnold Engineering Development Center.

[3] Waldron, H. F., "Viscous Hypersonic Flow over Pointed Cones at Low Reynolds Numbers," *AIAA Journal*, Vol. 5, No. 2, Feb. 1967, p. 208.

[4] Kussoy, M. I., "Hypersonic Viscous Drag on Cones in Rarefied Flow," TN D-4036, 1967, NASA.

[5] Whitfield, J. D. and Griffith, B. S., "Viscous Drag Effects on Slender Cones in Low-Density Hypersonic Flow," *AIAA Journal*, Vol. 3, No. 6, June 1965, pp. 1165–1166.

[6] Geiger, R. E., "Slender-Cone, Zero Angle-of-Attack Drag in Continuum and Noncontinuum Flow," Rept. R68SD15, Dec. 1968, General Electric Space Sciences Lab., Missile and Space Div.

[7] Kogan, M. N., "Hypersonic Flows of Rarefied Gases," *Journal of Applied Mathematics and Mechanics*, Vol. 26, No. 3, 1962, pp. 775–788.

[8] Laurmann, J. A., "Near Free Molecule Drag of a Cone in Hypersonic Flow," TM-537, Feb. 1967, Defense Research Corp.

[9] Ortloff, C. R., "Hypersonic Low Density Transitional Regime Flow Over Conical Vehicles," Rept. GRC TM-805, 1968, General Research Corp.

[10] Stewartson, K., "Viscous Hypersonic Flow Past A Slender Cone," *The Physics of Fluids*, Vol. 7, No. 5, May 1964, pp. 667–675.

[11] Ellinwood, J. W. and Mirels, H., "Axisymmetric Hypersonic Flow With Strong Viscous Interaction," Rept. TR-1001 (2240-10)-11, July 1967, Aerospace Corp.

[12] Mirels, H. and Ellinwood, J. W., "Viscous Interaction Theory for Slender Axisymmetric Bodies in Hypersonic Flow," *AIAA Journal*, Vol. 6, No. 11, Nov. 1968, pp. 2061–2070.

[13] Cunningham, B. E. and Kraus, S., "A 1-Foot Hypervelocity Shock Tunnel in Which High-Enthalpy, Real-Gas Air Flows Can be Generated With Flow Times of About 180 Milliseconds," TN D-1428, 1962, NASA.

[14] Loubsky, W. J., Hiers, R. S., and Stewart, D. A., "Performance of a Combustion Driven Shock Tunnel With Application to the Tailored-Interface Operating Conditions," *Proceedings of the Third Conference on Performance of High Temperature Systems*, Dec. 7–9, 1964.

[15] Hiers, R. S., Jr. and Reller, J. O., Jr., "Analysis of Nonequilibrium Air Streams in the Ames 1-Foot Shock Tunnel," TN D-4985, 1969, NASA.

[16] Geiger, R. E., "Some Sphere Drag Measurements in Low Density Shock Tunnel Flows," Rept. GE R63SD23, July 1963, General Electric.

[17] Bailey, A. B., "Sphere Drag Measurements in an Aero-Ballistics Range at High Velocities and Low Reynolds Numbers," TR-66-59, May 1966, Arnold Engineering Development Center.

[18] Masson, D. J., Morris, D. N., and Bloxsom, D. E., "Measurements of Sphere Drag From Hypersonic Continuum to Free-Molecule Flow," Research Memo RM 2678, Nov. 1960, RAND Corp.

[19] Feik, R. A., Genchi, A., and Vas, I. E., "A Study of Merging on Cones," *Proceedings of the Sixth Rarefied Gas Dynamics Symposium*, Boston, Mass., July 1968, to be published.

[20] Rakich, J. V., "Calculation of Hypersonic Flow over Bodies of Revolution at Small Angles of Attack," *AIAA Journal*, Vol. 3, No. 3, March 1965, pp. 458–465.

[21] Sentman, L. H., "Free Molecule Flow Theory and Its Application to the Determination of Aerodynamic Forces," TR 448514, Oct. 1961, Lockheed Missiles & Space Co.

[22] Vidal, R. J. and Bartz, J. A., "Surface Measurements on Sharp Flat Plates and Wedges in Low Density Hypersonic Flow," Rept. AF-2041-A-2, Feb. 1968, Cornell Aeronautical Lab.

[23] Horstman, C. C. and Kussoy, M. I., "Hypersonic Viscous Interaction on Slender Cones," *AIAA Journal*, Vol. 6, No. 12, Dec. 1968, pp. 2364–2372.